Nanostraw-Assisted Cellular Injection of Fluorescent Nanodiamonds via Direct Membrane Opening

Elke Hebisch, Martin Hjort, Diogo Volpati, and Christelle N. Prinz*

Due to their stable fluorescence, biocompatibility, and amenability to functionalization, fluorescent nanodiamonds (FND) are promising materials for long term cell labeling and tracking. However, transporting them to the cytosol remains a major challenge, due to low internalization efficiencies and endosomal entrapment. Here, nanostraws in combination with low voltage electroporation pulses are used to achieve direct delivery of FND to the cytosol. The nanostraw delivery leads to efficient and rapid FND transport into cells compared to when incubating cells in a FND-containing medium. Moreover, whereas all internalized FND delivered by incubation end up in lysosomes, a significantly larger proportion of nanostraw-injected FND are in the cytosol, which opens up for using FND as cellular probes. Furthermore, in order to answer the long-standing question in the field of nano-biology regarding the state of the cell membrane on hollow nanostructures, live cell stimulated emission depletion (STED) microscopy is performed to image directly the state of the membrane on nanostraws. The time-lapse STED images reveal that the cell membrane opens entirely on top of nanostraws upon application of gentle electrical pulses, which supports the hypothesis that many FND are delivered directly to the cytosol, avoiding endocytosis and lysosomal entrapment.

1. Introduction

Fluorescent nanodiamonds (FND) are nano-sized crystals containing color-centers arising from designed impurities in the crystal, such as nitrogen-vacancy centers. Due to their stable, non-blinking fluorescence and their minimal detrimental effects on cells, FND are expected to play a key role in biology

Dr. E. Hebisch, Dr. M. Hjort,[+] Dr. D. Volpati, Prof. C. N. Prinz
Division of Solid State Physics and NanoLund
Lund University
Lund 221 00, Sweden
E-mail: christelle.prinz@ftf.lth.se
Dr. M. Hjort,[+]
Navan Technologies Inc.
733 Industrial Rd, San Carlos, CA, United States

The ORCID identification number(s) for the author(s) of this article can be found under https://doi.org/10.1002/smll.202006421.

[+]Present address: Chemical Biology and Therapeutics, Lund University, 221 00 Lund, Sweden

and medical applications.[1–5] One prospect is to use them for long term cellular labeling and tracking.[6–9] In most reported studies, cells are exposed to FND by incubating them in a nanodiamond-containing cell medium. Whereas the number and fate of internalized FND varies from cell type to cell type, incubation with FND is not the most efficient delivery method for a given cell type. Indeed, when suspended in the cell medium, only few FND are internalized.[10,11] The internalization is achieved via endocytosis,[12] and most FND end up in endosomes and eventually lysosomes.[12–16] However, in order to take advantage of FND for labeling subcellular structures, they need to be able to interact with the biomolecules present in the cytosol. Direct microinjections of FND in zebrafish, Xenopus, and *Drosophila melanogaster* embryos, as well as in *Caenorhabditis elegans* intestinal cells allow the FND to avoid endosomal entrapment.[17–20] However, microinjections are only suitable for large cells. Alternatively, the nanofountain probe technology was used to deliver FND in the cytosol of individual cells for a variety of cell lines.[21] However, this method, together with the microinjection method, can only address one cell at a time. A more scalable strategy to avoid lysosomal entrapment consists of targeting an early endosomal escape after internalization via endocytosis. For instance, one group recently reported tuning the FND geometry in order to achieve an improved endosomal escape after incubating a cell with FND.[22,23] However, tuning or selecting the FND geometry is not straightforward and could represent a hurdle for researchers in biology and medicine, who mainly rely on commercially available FND or may not have access to electron microscopy for FND characterization. Dendrimers triggering endosomal escape have been used as delivery vectors for FND. For instance, maltotriose-conjugated polypropylenimine dendrimers have been used to deliver FND to subcellular protein assemblies, with the focus of demonstrating the potential of FND for correlative microscopy.[24,25] However, the proportion of internalized FND and the cell viability were not assessed. The latter point is especially important since concerns have been raised about the cytotoxicity of maltotriose-conjugated polypropylenimine dendrimers.[26] Therefore, whereas delivering FND using these dendrimers may be a valid method for performing correlative microscopy, it might not be optimum to achieve delivery in a great number of cells without affecting their function. Finally, electroporation

**ADVANCED
SCIENCE NEWS**
www.advancedsciencenews.com

NANO · MICRO

small
www.small-journal.com

has also been tested to deliver FND to the cytosol, however, resulting in poor cell viability.[27,28] Therefore, there is a pressing need for achieving highly efficient delivery of FND directly to the cytosol of multiple cells without detrimental effects on the cell viability.

Here, we use nanostraws to inject FND directly to the cytosol. Nanostraws are inorganic nanotubes protruding from a cell culture-compatible polymer membrane. Nanostraws are capable of injecting a wide range of biomolecules into living cells cultured on top of the nanostraw membrane, without perturbing cellular function or viability.[29,30] For large molecules, the transport through the nanostraws is electrokinetically enhanced by applying a gentle, low-power, low-voltage electrical field across the nanostraw membrane.[31–33] The injection process is thought to come from the opening of nanosized pores in the cell membrane upon the application of the electric field, although this has not been directly demonstrated yet.[32]

In our case, we used nitrogen-vacancy FND, because of their red fluorescence, harmless to cells and tissues, and their amenability to superresolution optical microscopy using stimulated emission depletion (STED) microscopy.[34] The FND injections were performed by culturing cells on top of nanostraws and by applying a series of low voltage DC pulses across the nanostraw membrane, driving the FND, which are in suspension in the reservoir underneath, inside cells. With this direct delivery method, in just a few seconds, we inject more FND inside cells than when incubating cells for 24 h in an FND-containing medium. Moreover, in the case of nanostraw-assisted injections, most FND are located in the cytosol and not in lysosomes. STED live-cell imaging revealed that the cell membrane on top of nanostraws opens completely upon the application of the DC pulses, which answers a key question in the field regarding the nature of the cell-nanostraw interface.

2. Results and Discussion

2.1. Characterization of the FND

The FND were purchased from Adámas Nanotechnologies (NDNV30nmHi30ml, made by milling, with a nominal average diameter of 30–35 nm, Adámas Nanotechnologies, USA), and were characterized in our laboratory using scanning electron microscopy (SEM), dynamic light scattering (DLS), and electrophoretic light scattering (see Supporting Information for detailed experimental protocol). SEM images show that the FND are irregular in shape; dynamic- and electrophoretic light scattering measurements yielded an average FND diameter of 40 nm and a ζ-potential of −34.4 mV in dilute phosphate buffered saline ($0.1 \times$ PBS) at 37 °C, which is the medium in which FND are suspended during intracellular delivery (**Figure 1**; Table S1, Supporting Information). In the cell culture medium, we measured a fivefold increase in FND size and a ζ-potential of −10 mV, which is due to a combination of the absorption of various proteins on the FND and to the increased salt concentration in the cell culture medium, screening the charges and inducing FND aggregation.[35]
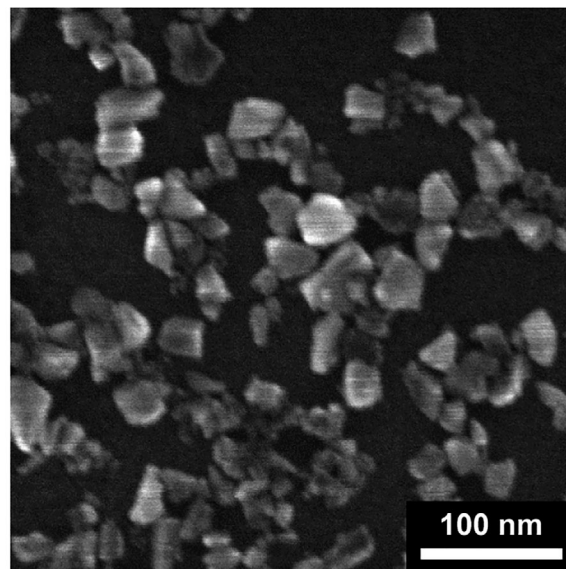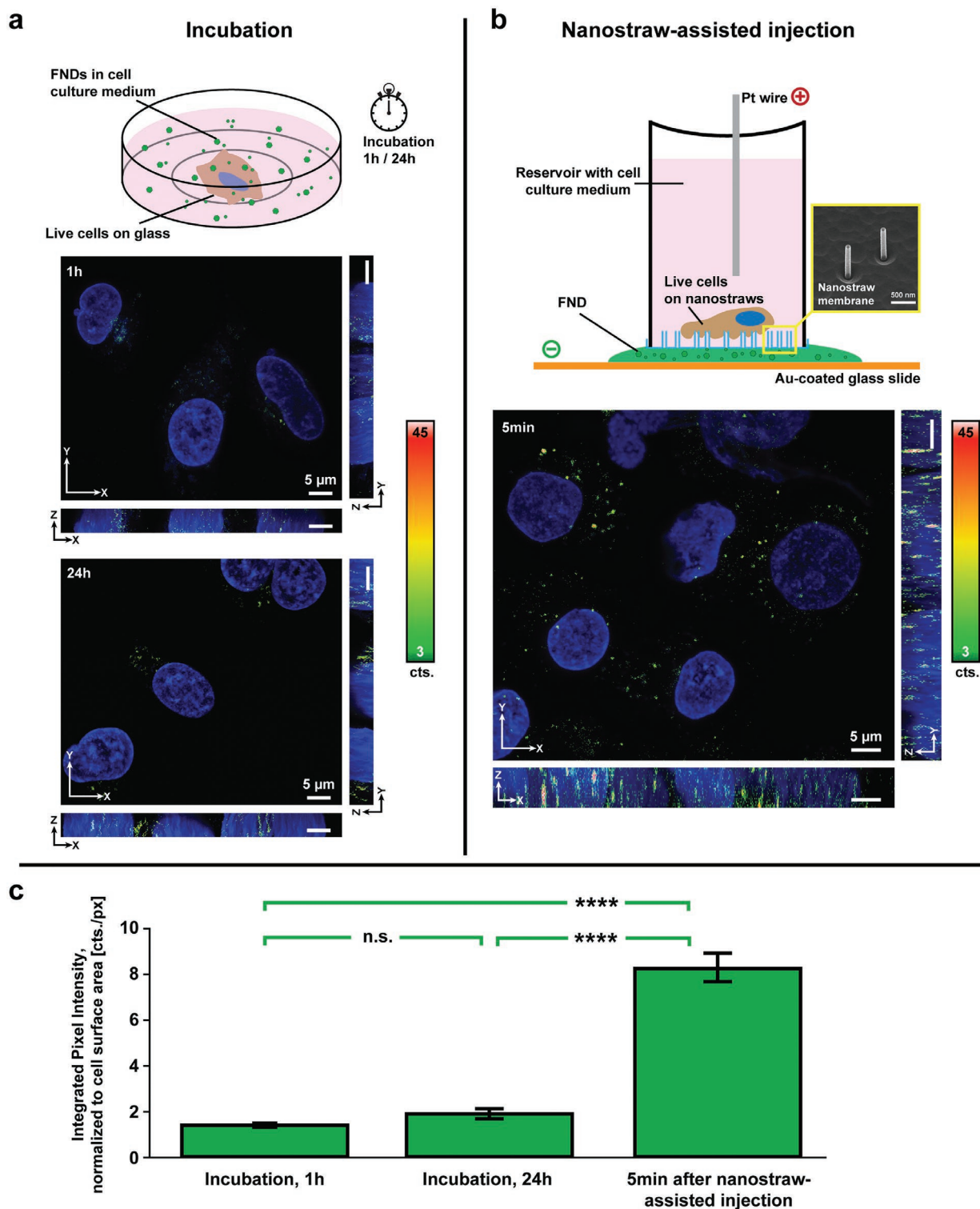

Figure 1. SEM image of the FND used in this study.

2.2. Nanostraw-Injection Results in Five Times More FND Delivered Inside Cells

Nanostraws were fabricated from commercially available polycarbonate (PC) and polyethylene terephthalate (PET) track-etched membranes (see Experimental Section for detailed experimental protocol). Briefly, the membranes were coated with a 10 nm aluminum oxide layer, deposited using atomic layer deposition (ALD) (Cambridge NanoTech Savannah 100). The topmost Al_2O_3 layer was etched anisotropically, followed by a selective etch of the polymeric membrane, resulting in nanostraws protruding from the substrate. The nanostraws used in this study had an inner diameter of ≈80 nm, an outer diameter of ≈100 nm and a length of ≈1 µm, with a density of ≈$2–5 \times 10^7$ cm^{-2} (Figure S1, Supporting Information).

We compared nanostraw-assisted FND injections to cell incubation in an FND-containing medium, which is the most commonly used method for transporting FND into cells (**Figure 2**a,b), see Experimental Section for detailed experimental protocol.

In order to inject FND inside cells using the nanostraws, custom made nanostraw devices were prepared by gluing the nanostraw membrane to a polymer cylinder (see Experimental Section for detailed experimental protocol). A549 cells were cultured on the nanostraw substrate for 18 h. For injection, the cell-nanostraw device was placed on top of a gold-coated microscope slide on which a 20 µl droplet of 100 µg ml^{-1} FND in $0.1 \times$ PBS had been deposited. A Pt electrode was dipped in the cell medium, on top of the cells and electrical pulses were applied across the nanostraws (two series of square electrical pulses of 25 V at 20 Hz with a pulse duration of 100 µs were applied for 20 s each, 2 min apart). The electrical pulses are thought to result in local cell membrane destabilization and electrokinetically enhanced transport of the FND to the cytosol.[31] We verified that the cell viability is not affected by the nanostraw-assisted FND delivery (Figure S2, Supporting

**ADVANCED
SCIENCE NEWS**

www.advancedsciencenews.com

NANO · MICRO

small

www.small-journal.com

Figure 2. Fast and high-efficiency intracellular delivery of FND via nanostraw-assisted injection, in comparison to low-yield FND delivery by incubation. a) Top panel: Schematics of the intracellular FND delivery via incubation. Middle and bottom panel: Confocal fluorescence microscopy images (*xy*, *xz*, and *yz* scans) of live A549 cells after 1 and 24 h of incubation in FND-containing medium. b) Top panel: Schematics of nanostraw-assisted FND injections. Bottom panel: Confocal fluorescence microscopy image of live cells on nanostraws imaged 5 min after FND delivery. In all images, the FND signal is shown in green-yellow-red, depending on the pixel intensity, and the cell nucleus signal is shown in blue. All images are 2D projections of the maximum pixel intensity obtained from 3D (XYZ) sample scans. For all images, the background noise corresponds to three counts. c) Quantification of the internalized FND signal: Integrated FND pixel intensity normalized to cell area (±S.E.M.) assessed for the two FND delivery methods presented in (a) and (b). n.s.: $p > 0.05$; ****: $p \leq 0.0001$, two-sided Mann–Whitney–Wilcoxon U Test.

**ADVANCED
SCIENCE NEWS**

www.advancedsciencenews.com

**NANO · MICRO
small**

www.small-journal.com

Information). After FND delivery, the nanostraw substrate was gently detached from the polymer tube, rinsed in a cell imaging medium, then placed upside-down on a drop of the cell imaging medium deposited on a glass cover slip and imaged using confocal microscopy to assess cellular FND internalization. In the case of delivery via incubation, cells were incubated on a glass bottom petri dish in an FND-containing cell medium (100 µg ml^{-1}), for 1 and 24 h (Figure 2a) and subsequently imaged using confocal microscopy to assess FND internalization.

The results show that cells incubated for 1 and 24 h in an FND-containing medium had very few internalized FND (Figure 2a–c; Figure S3, Supporting Information). In contrast, many FND were observed in cells after nanostraw injections, as shown by the higher pixel intensity and higher positive pixel counts for FND signal (Figure 2b,c; Figure S3, Supporting Information). After integrating the FND pixel intensity and normalizing it to the total cell area (estimated from the corresponding bright field images), we found that the FND signal inside cells 5 min after nanostraw-injection is approximately fivefold higher than the FND signal after 1 and 24 h incubation. This shows that nanostraw-injection of FND is a very efficient method to deliver FND into cells.

2.3. Most Nanostraw-Injected FND Are Not Entrapped in Lysosomes

Since entrapment in cell compartments, such as endosomes and lysosomes, is a reported issue when performing cell delivery, we assessed the spatial distribution of FND with respect to lysosomes, which we assume to collect all FND internalized via the endocytic pathway. Cells were stained for Lysosomal-Associated Membrane Protein 1 (LAMP1), and confocal microscopy was used to assess the colocalization of FND and LAMP1 for both FND delivery methods. In the case of incubation with an FND-containing medium, confocal microscopy images show that the few internalized FND are located inside lysosomes (**Figure 3**a,b,e) with ≈90% and ≈83% of the pixels that are positive for FND signal being also positive for LAMP1 signal, for 1 and 24 h incubation periods, respectively. In contrast, nanostraw-injected FND were found outside lysosomes (Figure 3c,d,e), with only ≈33% and ≈43% of the pixels that are positive for FND signal being positive for LAMP1, 1 and 24 h after injection, respectively. This shows that a majority of the nanostraw-injected FND do not end up in lysosomes. The proportion of FND signal not colocalized with the lysosomal signal increases slowly from 33% to 43% over 24 h, which suggests that most FND that are not entrapped in cellular compartments at the time of injection remain so and are not quickly transported to lysosomes. This indicates that 60–70% of the injected FND avoid lysosomal entrapment and may be located in the cytosol, where they could interact with biomolecules and organelles, which opens up for long time live imaging of cell components. By avoiding lysosomal entrapment to a great extent, the nanostraw injection method will be of great interest in the field of drug delivery, where lysosomal entrapment is a tremendous problem.[36,37]

Note that the apparent colocalization of FND with the nucleus fluorescence in Figure 3d is due to the maximal pixel intensity projection representation of the image. In fact, the ensemble of individual z-slice images used in Figure 3d shows that FND do not penetrate the nucleus (Figure S4, Supporting Information).

Besides lysosomal entrapment, we have found a few reports in the literature where FND and other cargos such as molecular beacons accumulate at mitochondria.[13,38] To assess whether such an accumulation could take place in the present case, the mitochondria were stained. The results show that, for both incubation and nanostraw-assisted injections, the FND signal does not colocalize with the mitochondria signal (Figure S5, Supporting Information).
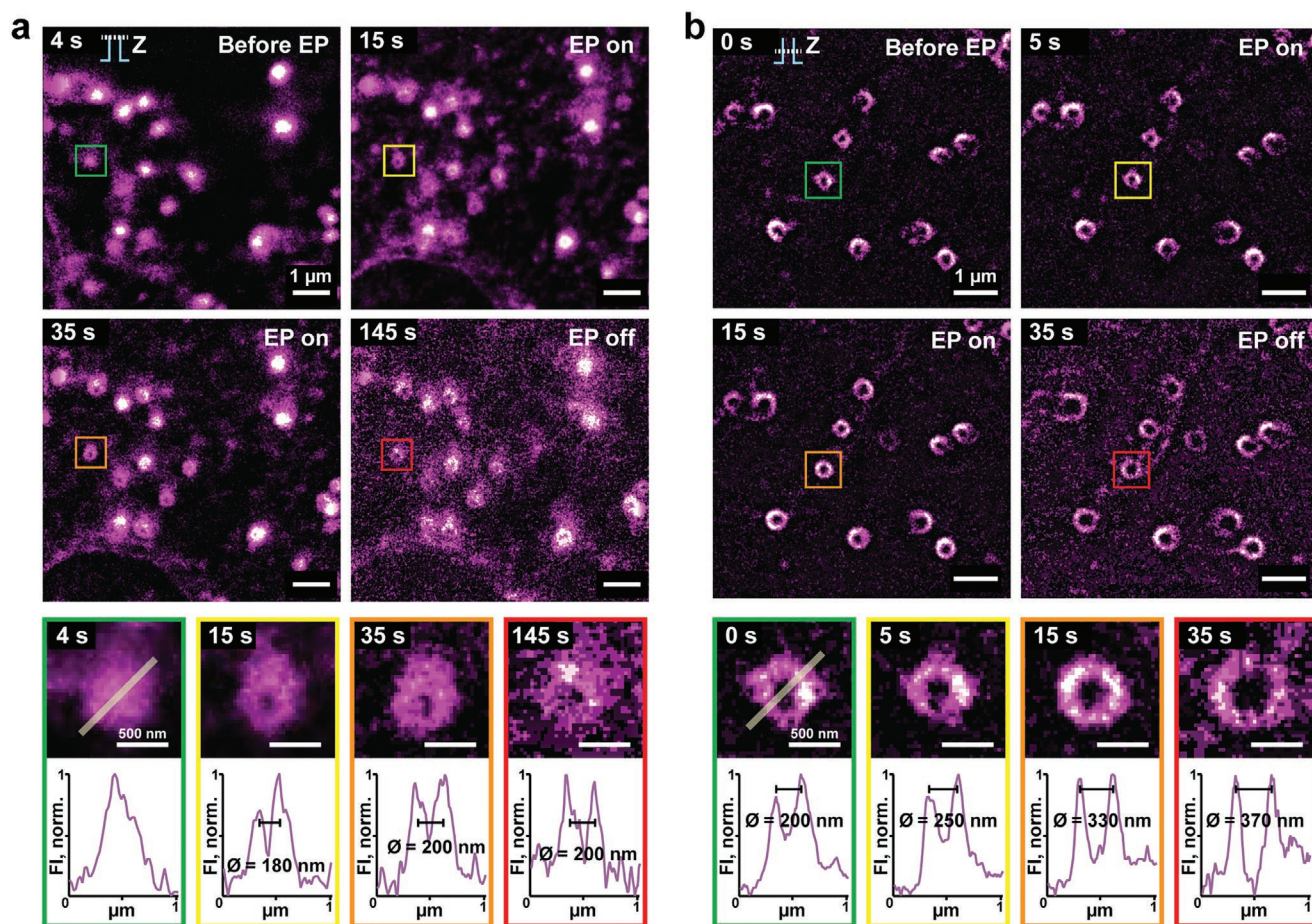
It is surprising that some of the FND signal colocalizes with the lysosome signal when using the nanostraws for intracellular delivery. A possible explanation could be that FND are not actually inside lysosomes but simply in close proximity to lysosomes, at a distance which is shorter than the resolution of confocal microscopy. However, by simulating a random signal distribution for FND and lysosomes, and comparing the resulting colocalization with the experimental one, we could show that the extent of colocalization of the FND signal and the lysosomal signal is not the result of a random process (Figure S6, Supporting Information). The possible presence of FND inside lysosomes after nanostraw-assisted injection could possibly be explained by the fact that, on nanostraws not covered by cells, FND are transported to the cell medium where they can be internalized via endocytosis. Another possibility to explain the presence of FND in lysosomes is a type of autophagy process, where the cell would detect intracellular FND and encapsulate them for destruction.[39] However, in such a case, one would expect that the number of FND encapsulated in lysosomes would increase dramatically with time, which is not the case. Performing a live-cell, time-lapse imaging of lysosomes and FND during delivery could possibly shed light on the dynamic of FND encapsulation by following the fate of individual FND after intracellular delivery.

2.4. Live STED Imaging of the Cell Membrane upon Application of the Electrical Pulses

A long-time debate in the field of using nanostructures to transport cargos in cells concerns the state of the cell membrane. Different mechanisms are proposed to explain the efficient delivery yields achieved by nanostraws. One possibility would be the increase in membrane permeability due to the imposed curvature.[40] Another possibility would be the piercing of the cell membrane by the nanostraws. However, spontaneous piercing of the cell membrane by nanostraws has been shown to occur very seldom.[41,42] On the other hand, the use of electrical pulses is known to greatly enhance delivery efficiencies.[31,32] The enhanced delivery efficiency is thought to be due to local electroporation, creating nanoscaled pores on the cell membrane regions interfaced with nanostraws. Whether the membrane opens nanopores or opens up entirely on top of the nanostraws upon the application of the electrical pulses remains unknown. In order to assess the state of the cell membrane on top of the nanostraws, we used STED microscopy and the cholesterol-based cell membrane label, Chol-KK114,
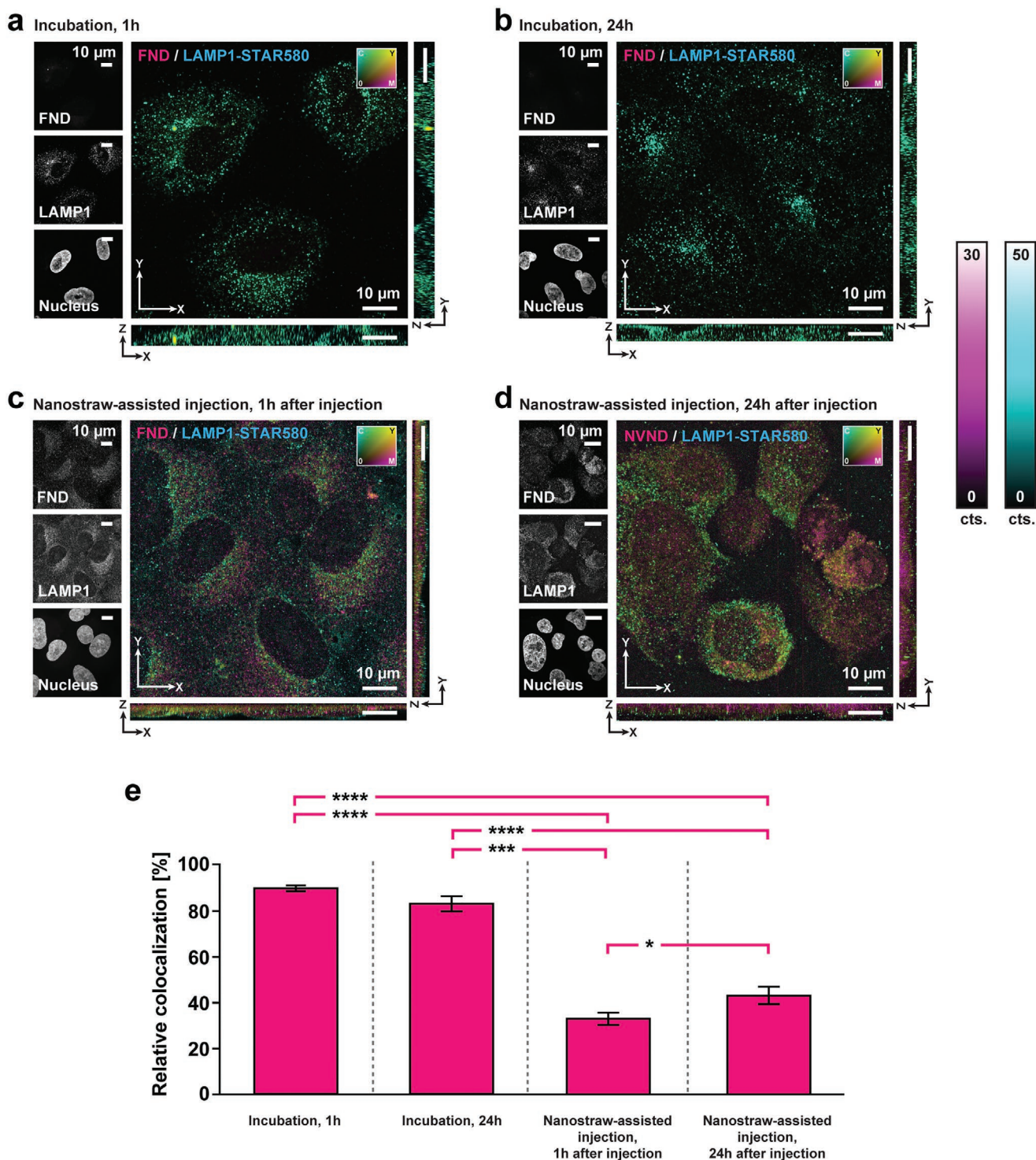
Figure 3. Nanostraw-assisted injection of FND yields decreased lysosomal trapping of FND. Colocalization of FND and lysosome (LAMP1) fluorescence signals in confocal microscopy images of cells. a,b) Representative confocal images of cells incubated with FND-containing cell medium for 1 and 24 h, respectively. c,d) Confocal microscopy images of cells 1 and 24 h after nanostraw-assisted FND delivery, respectively. In all images, the FND signal is shown in magenta, normalized to (0–30) pixel counts and the lysosome signal is shown in cyan, normalized to (0–50) pixel counts. The displayed images are 2D projections of the maximum pixel intensity obtained from 3D (XYZ) sample scans; maximum pixel intensity projections along the respective third scanning axis of each image are shown. Single-color images of the FND, lysosome, and nuclear signal channels are displayed on the left of each two-color overlay image. e) Relative colocalization of the FND signal with the lysosomal signal with respect to the total FND signal (± S.E.M.). *: $p \leq 0.05$; ***: $p \leq 0.001$; ****: $p \leq 0.0001$, two-sided Mann–Whitney–Wilcoxon U Test.

**ADVANCED
SCIENCE NEWS**

www.advancedsciencenews.com
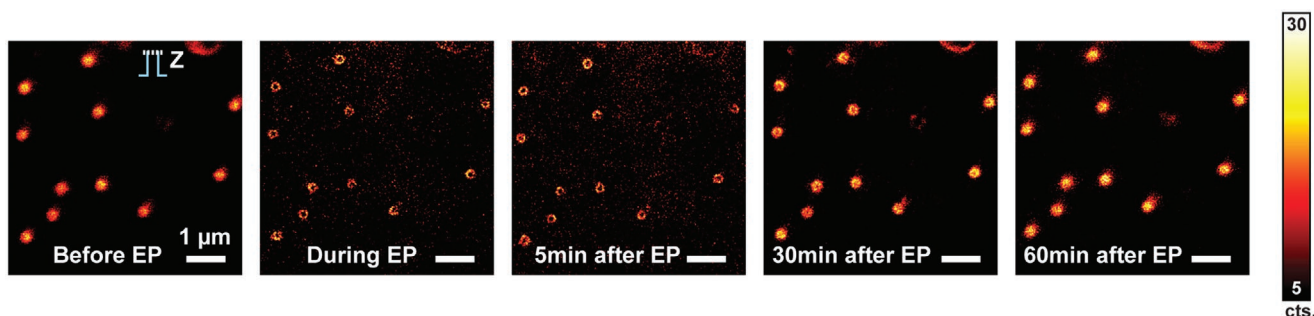
NANO · MICRO

small

www.small-journal.com

Figure 4. Mechanisms of nanostraw-assisted intracellular delivery: The cellular membrane opens up and widens around nanostraws upon electroporation. STED micrographs of the membrane of live A549 cells on nanostraws before, during, and after the application of low-voltage electrical pulses (EP) through the nanostraws. a) STED microscopy images of the membrane of living cells on nanostraws at four different time points (t = 4, 5, 35, and 145 s from the beginning of the image acquisition) of a series of scans acquired at 1 fps and recorded in a focus-locked focal plane set at the tip of the nanostraws (as indicated schematically in the top left panel). Square electrical pulses (25 V, 20 Hz, 100 μs pulse duration) were applied from t = 5 s to t = 35 s. Bottom panels: Close-up view of the membrane signal around one nanostraw and the corresponding normalized fluorescence intensity (FI, norm.) profile across the nanostraw, taken at t = 4, 5, 35, and 145 s. b) STED microscopy images of the membrane of living cells on nanostraws at four different time points (t = 0, 5, 15, and 35 s from the beginning of the image acquisition) of a series of scans acquired at 1 fps and recorded in a focus-locked focal plane set to the middle of the nanostraws (as indicated schematically in the top left panel). Square electrical pulses (25 V, 20 Hz, 100 μs pulse duration) were applied from t = 5 s to t = 25 s. Bottom panels: Close-up view of the membrane signal around one nanostraw and the corresponding normalized fluorescence intensity (FI, norm.) profile across the nanostraws at the four time points. All images were smoothed using a low-pass Gaussian filter.

which labels the membrane homogeneously[43,44] (Figure S7, Supporting Information). The confocal fluorescence signal corresponding to the cell membrane is higher at the nanostraw location (Figure S8, Supporting Information). This increase in fluorescence is due to the cell membrane following the contours of the nanostraws, as shown in the STED images, where the membrane signal forms a ring around the nanostraws at mid-height (**Figure 4**b top-left panel; Figure S8, Supporting Information) and a disk on top of the nanostraws (Figure 4a top-left panel).

In order to assess the effect of the electrical pulses on the cell membrane, two sets of STED time lapse images were acquired at a rate of 1 fps, one with the focal plane set at the tip of the nanostraws (Figure 4a) and one with the focal plane set around the middle of the nanostraws (Figure 4b). Square electrical pulses were applied across the nanostraw membrane, from t = 5 s to t = 35 and 25 s, for Figure 4a,b, respectively. Before the application of the electrical pulses, the cellular membrane appears continuous, with the membrane fluorescence signal forming a full disk on top of the nanostraws (Figure 4a; Movie S1, Supporting Information). When the electric field is turned on, the membrane opens gradually, eventually forming a pore of similar dimensions to the ones of the nanostraws. When the electric field is turned on, the membrane is also moving away from the nanostraw side walls, as shown by the increase in diameter of the membrane signal from 200 to 370 nm (Figure 4b; Movie S2, Supporting Information). Both the membrane pore opening and the increased distance of the membrane to the nanostraw walls appear stable after switching off the electrical field, at least on the timescale of our experiments.

**ADVANCED
SCIENCE NEWS**

www.advancedsciencenews.com

NANO · MICRO

small

www.small-journal.com

Figure 5. Cell membrane recovery on nanostraws after the application of electroporation pulses. STED micrographs of the membrane of live A549 cells on top of nanostraws before, during, 5, 30, and 60 min after the application of low-voltage EP through the nanostraws. The membrane pores start to close after 30 min and are completely closed 60 min after switching off the EP.

In previous studies where conductive nanowires were used to measure cardiomyocyte action potentials, the measurements showed that the application of electrical pulses to the nanowires lead to a transition from extracellular measurements to intracellular measurements, suggesting the formation of pores in the membrane around the nanowires.[45] This transition was reversed ≈10 min after switching off the electrical pulses, suggesting a recovery of the membrane on this timescale. In order to investigate whether the membrane closes again on the nanostraws after the application of the electrical pulses, we imaged the membrane on nanostraws using STED microscopy every 5 min. Representative time lapse images of the membrane recovery are shown in **Figure 5**. The membrane forms a continuous disk on top of the nanostraws and opens up when the electrical pulses are applied. The membrane pores start to close 30 min after turning off the electrical pulses and are completely closed 60 min after turning off the electrical pulses. The reversibility in the membrane pore opening when using nanostraw-assisted injection supports claims that nanostraw injection does not have any detrimental effect on the cell. This is further supported by the fact that cells remain viable on nanostraws 24 h after the application of electrical pulses (Figure S2, Supporting Information), and by previous investigations showing very few changes in gene expression after nanostraw injections.[29,30]

Interestingly, our results show the formation of membrane pores that are more than an order of magnitude larger than that predicted by the Smoluchowski equation.[46,47] Similarly, the resealing of the membrane is much slower in the present case (30–60 min), than what has been shown in the case of nano-fountain probe electroporation (few tens of seconds).[48] We can possibly attribute these differences to longer electroporation pulses and a higher number of pulses, as it has been shown that both the membrane pore size and the resealing time increases with the number of pulses and pulse duration.[49] Increase in the local electrical field and increased membrane tension on nanostraws may also be an explanation.[47,50]

In previous studies, the dynamics of the permeabilization of the membrane by nanostraws and nanowires has been assessed by either monitoring the successful delivery of cargos[29,42,51] or by the intra- and extracellular signature of the measured action potential signal in the case of electrophysiology measurements.[45] Snapshots of the cell membrane have also been provided using fluorescence and electron microscopy,[52–55] which have been used to confirm the presence of

a membrane around the nanostructures. However, using these methods, it can be difficult to interpret the lack of a membrane signal, especially when it comes to determining the size and shape of the membrane opening. Therefore, until today, there was an uncertainty regarding the nature of membrane permeabilization upon the application of electroporation pulses. Our time lapse movies provide a direct visualization of the state of the cell membrane upon the application of electrical pulses and show that the membrane opens completely on top of the nanostraws. This broad opening explains the high efficiency in FND delivery, and is a prerequisite for achieving intracellular delivery of large constructs.

3. Conclusion

In summary, we demonstrate the superiority of nanostraw-assisted delivery of FND into A549 cells over delivery achieved through incubation. A series of electrical pulses is applied across the nanostraw substrate to facilitate the transport of FND inside cells. Using this method, over five times more FND can be delivered intracellularly in just a few minutes, compared to when using incubation, where only few FND can be found inside cells after up to 24 h incubation in an FND-containing medium. Whereas the very few FND delivered via incubation are all trapped in lysosomes, 60% to 70% of the FND delivered using the nanostraws are not located in lysosomes, which opens up for interactions with intracellular organelles/biomolecules and long term intracellular labeling using FND. Video-rate STED images revealed that the membrane opens completely on top of the nanostraws upon the application of the electrical pulses. The membrane recovers and pores are closed again 1 h after the application of the electrical pulses. The large membrane opening that we observed is a prerequisite for the delivery of large cargos inside cells, thereby greatly expanding the usability of nanostraws within life science applications.

4. Experimental Section

Fluorescent Nitrogen-Vacancy Nanodiamonds (FND): Carboxylated 30 nm red fluorescent nitrogen-vacancy nanodiamonds (FND) in DI water were purchased from Adámas Nanotechnology (NDNV30nmHi10ml, Adámas Nanotechnologies, Raleigh, NC, USA). According to the supplier, the FND have an average diameter of

**ADVANCED
SCIENCE NEWS**

www.advancedsciencenews.com

NANO · MICRO

small

www.small-journal.com

30–35 nm, a fluorescence lifetime of $\tau = 13$ ns, and show fluorescence with peak excitation/emission maxima of (570/680) nm.

Determination of the Size and Zeta Potential of the FND: The size of FND, determined via DLS, and the Zeta potential (ζ-pot.) of FND, determined via electrophoretic light scattering, were assessed using a Zetasizer Nano ZS (Malvern Panalytical Ltd., Malvern, UK), equipped with a 4 mW He-Ne laser (632.8) nm. Dilutions of each 100 µg ml^{-1} FND were prepared in DI water, 0.1 × PBS, and in full F-12K cell culture medium, composed of F-12 K medium (21127022, Gibco, Life Technologies), supplemented with 10% Fetal Bovine Serum (FBS, Sigma Aldrich) and 1% Penicillin-Streptomycin (P4333, BioReagent, Sigma Aldrich). The FND dilutions were sonicated for 15 min immediately prior to being loaded into DTS1070 disposable folded capillary cells (DTS1070, Malvern Panalytical Ltd., Malvern, UK) and transferred into the Zetasizer. The size and ζ-pot. measurements of FND were performed at 25 and 37 °C; size measurements were always performed before electrophoretic mobility measurements. The size measurements via DLS were performed using backscattering at a fixed scattering angle of $\theta = 173°$ and using the "General purpose" analysis model built into the Zetasizer Nano ZS software to solve the Stokes–Einstein equation. The electrophoretic mobility measurements were carried out at $\theta = 17°$ and using the Smoluchowski approximation (F(ka) = 1.5) to solve the Henry F(ka) equation.

Two samples were prepared for each FND dilution and three measurement runs per sample were performed for both the size measurement and the measurement of the ζ-pot. at each temperature (25 and 37 °C).

Scanning Electron Microscopy Imaging of the FND: For SEM imaging, FND in stock solution were washed twice in ethanol and once in isopropanol, using centrifugation (2000 RCF during 10 min) to sediment the nanoparticles and sequentially remove the supernatant. After washing, FND were re-suspended in IPA and drop-casted on a silicon substrate. The substrates with FND were placed on a hot plate at 55 °C for 60 min for solvent evaporation. SEM images were acquired using a Hitachi SU8010 SEM with an acceleration voltage set to 20 kV and low angle backscattered electrons in the upper detector, which gives both topographical information and compositional contrast.

Nanostraw Fabrication: *From PC membranes*: Track-etched PC (IT4IP S.A.) with 2.0×10^7 pores/cm^2 and pore size 100 nm were cleaned in an isotropic O$_2$ barrel plasma etcher for 30 s (Diener electronic). After cleaning, the membrane was coated with 10 nm Al$_2$O$_3$ by ALD (Cambridge NanoTech Savannah 100). To cover all membranes including the inner part of the nanopores, pulse cycles of 15 ms were employed for trimethylaluminum and H$_2$O, with 45 s resting time between pulses, for a total of 100 pulses. After ALD deposition, the Al$_2$O$_3$ coated polycarbonate membrane was etched anisotropically in two steps (APEX SLR F-based ICP-RI-Plasma-Therm). First, the topmost Al$_2$O$_3$ layer was etched using an Ar gas flow of 40 sccm, ICP 400 W and RF 60 W for 150 s. In the second step, the polymeric membrane was selectively etched to expose the Al$_2$O$_3$ nanostraws with a gas composition of 45 sccm of O$_2$ and 5 sccm of SF6, IPC 400 W and RF 50 W for 90 s.

From PET membranes: 12 µm thick track-etched PET membranes (GVS Filter Technology, Sanford, ME, USA) with 100 nm diameter pores and a pore density of 3×10^7 pores/cm^2 was coated with 10 nm Al$_2$O$_3$ in an ALD reactor (Savannah S100, Cambridge Nanotech, Waltham, MA, USA) using trimethylaluminum and water as precursor gases and an ALD reactor temperature of 100 °C. After coating, the top layer Al$_2$O$_3$ was removed using Argon-based inductively coupled plasma reactive ion etching (ICP-RIE) in an Apex plasma etcher (Plasma-Therm, Saint Petersburg, FL, USA), using 100 W RF and 250 W inductively coupled plasma reactive ion etching for 2 min. Nanostraws were formed by oxygen-based RIE in the same reactor using 25 W RF 500 W ICP for 90 s.

SEM Imaging of the Nanostraws: For SEM imaging of the nanostraws, small pieces of the nanostraw membranes were coated with 4 nm of Pt/Pd using sputtering (Quorum Q150T ES, Quorum Technologies Ltd., Laughton, UK) at a deposition rate of 2 nm min^{-1}. SEM images were acquired in a Hitachi SU8010 SEM with acceleration voltage set to 15–20 kV and using the secondary electrons upper and lower detectors.

Cell Culture: Human lung adenocarcinoma A549 cells were purchased from the European Collection of Authenticated Cell Cultures (ECACC via Sigma Aldrich/Merck). After thawing, cells were seeded at a density of 5000 cells/cm^2 in T25 cell culture flasks (Nunc, 156367, via Thermo Fisher Scientific) and cultured in full F-12K cell culture medium at 37 °C under 5% CO$_2$ atmosphere. Cells were passaged when reaching about 80–90% confluency, as reported previously.[56]

Incubation of Cells with FND Suspended in the Cell Medium: Prior to exposure to nanodiamonds, cells were seeded at a density of 6000 cells/cm^2 in glass-bottom Petri dishes (P35G-1.5-20-C, MatTek Corporation, Ashland, MA, USA) and cultured for 18 h in full F-12K cell culture medium. After 18 h of cell culture in glass-bottom Petri dishes, the cell culture medium was removed and replaced with 500 µl fresh cell culture medium containing 100 µg ml^{-1} FND. Cells were incubated with FND for 1 or 24 h, as specified in the main text, and subsequently prepared for either live confocal/STED microscopy imaging as described below or prepared for indirect immunofluorescence staining targeting LAMP1. Five samples per scenario (1 or 24 h incubation) were prepared for live cell imaging; between three to five images per sample were recorded and analyzed; each image covered a region of interest (ROI) containing on average four individual cells. Three samples per scenario (1 or 24 h incubation) were prepared for indirect immunofluorescence staining for LAMP1; three images per sample were recorded and analyzed; each image covered a ROI containing on average four individual cells.

Nanostraw-Assisted Intracellular Delivery of FND: For the construction of nanostraw devices for FND delivery, plastic cylinders (Ø_outer ≈10 mm; Ø_inner ≈7 mm; height ≈10 mm) were designed and 3D printed in house using a Formlabs Form 2 3D printer (Formlabs Inc., Somerville, MA, USA) and the standard Formlabs clear photopolymer resin (RS-F2-GPCL-04, Formlabs Inc.). Nanostraw devices were assembled by gluing nanostraw membranes to the polymer cylinders using biocompatible double sided tape (467MP 200MP Adhesive, 3M, St. Paul, MN, USA), such that the nanostraws protruded into the cylinders. Cells were seeded at a density of 6000 cells/cm^2 onto the nanostraws and cultured for 18 h in full F-12K cell culture medium inside 24-well-plates, with full F-12K cell culture medium surrounding the nanostraw devices. After 18 h of culturing, the nanostraw devices with the cells were placed onto a drop of ca. 20 µl of 100 µg ml^{-1} FND in 0.1 × PBS deposited on a gold coated glass slide (100 nm Au thickness, 643246, Sigma Aldrich). The authors used 0.1 × PBS as a dilution medium for the FND in order to limit the current flow through the circuit (and thus minimizing cell damage), while keeping a stable current flow and avoiding osmotic shock. As the positive electrode, a platinum wire was placed inside the nanostraw device cylinder (filled with full F-12K cell culture medium). Conductive tape was stuck onto the gold coated glass slide, which was used as the negative electrode. The electrodes were connected to a pulse generator (TGP110, Aim and Thurlby Thandar Instruments, Huntingdon, UK) in series with a signal amplifier (WMA-300, Falco Systems BV, Katwijk aan Zee, The Netherlands). The electrodes were placed 1 mm apart using a micromanipulator. Square electrical pulses of 25 V, at a frequency of 20 Hz, and with a pulse duration of 100 µs were applied between the electrodes in two steps of 20 s each, with 2 min resting time in between. The properties of the generated electrical pulses were controlled using an oscilloscope; the electrical current during the electroporation step was ca. 40 mA.

After the low-voltage electroporation step, cells were either directly stained for their nuclei using Hoechst33342 (as described below) and imaged, or fixed and stained for lysosomes (via indirect immunofluorescence targeting LAMP1) 1 or 24 h after electroporation.

Five samples were prepared for live cell imaging 5 min after nanostraw-assisted injection; between three to five images per sample were recorded and analyzed; each image covered a ROI containing on average four individual cells. Three samples for the scenarios of 1 and 24 h after nanostraw-assisted injection were prepared for indirect immunofluorescence staining for LAMP1; three images per sample were recorded and analyzed; each image covered a ROI containing on average four individual cells.

Assessment of Cell Viability: The cell viability was assessed to determine the influence of the low-voltage electroporation FND-delivery step on the cells. Cells were seeded at a density of 6000 cells/cm² on PC nanostraws in prepared nanostraw devices (for the preparation of nanostraw devices, refer to the above section). Cells were either cultured on the nanostraws for 42 h, or were cultured on the nanostraws for 18 h, at which time FND were delivered to the cells using the nanostraws (as described above), and cultured for another 24 h. Cells were subsequently stained with the LIVE/DEAD Viability/Cytotoxicity Kit for mammalian cells (L3224, Molecular Probes, Thermo Fisher), using a staining solution of 4 µm EthD-1 and 2 µm Calcein AM (prepared in Dulbecco's Phosphate Buffered Saline, without calcium or magnesium, 14190169, Gibco, Thermo Fisher), with an incubation time of 5 min at room temperature, in the dark. Cells were washed once in DPBS and successively stained for their nuclei using Hoechst33342 at a concentration of 2.5 µg ml⁻¹ (in DPBS) and with an incubation time of 2 min, at room temperature, in the dark. Cells were washed twice in DPBS; the nanostraw membrane was gently removed from the nanostraw device, mounted onto a drop of the LIVE/DEAD working solution, and imaged using a custom-built upright fluorescence microscope. Three samples per scenario (42 h culture or 18 h + 24 h culture including the nanostraw-assisted electroporation step) were prepared, five individual ROI of an area of ca. (220 × 220) µm² were recorded per sample in three single color channels, that is, exc/em at 375 nm/(430/40) nm for Hoechst33342 indicating all cells, exc/em at 470 nm/(515/30) nm for Calcein AM indicating live cells, and exc/em at 555 nm/(595/30) nm for EthD-1 indicating dead cells.

A brightness threshold for the single color channel images per ROI was set using the custom-written MATLAB routine described in the section about data analysis. Cells in the binarized single color channel images were counted using the built-in function "Analyze Particles" in the software Fiji (http://imagej.net/Fiji). Cell viability was determined as the fraction of cells that showed a positive Calcein AM signal while at the same time showing a negative EthD-1 signal of all (Hoechst33342-positive) particles.

Fluorescence Labeling of Live Cells: *Cell membrane*: Live A549 cells were adherent during all of the fluorescence labeling protocols described in the following. The cellular membrane was stained using the fluorescent cholesterol analog Cholesterol-PEG-KK114 (Chol-KK114, courtesy of Dr. Vladimir Belov of the Max Planck Institute for Biophysical Chemistry in Goettingen, Germany).[43] Cells were labeled at a Chol-KK114 concentration of ≈25 mm (prepared in the full F-12K cell culture medium) and with an incubation time of 2 min (at room temperature). Cells were subsequently washed twice in a cell imaging medium.

Immediately before live-cell imaging, all live A549 cell samples (except for the membrane-labeled cells on nanostraws used for video-rate STED imaging) were stained for cell nuclei using Hoechst33342 (62249, Thermo Fisher Scientific), at a concentration of 2.5 µg ml⁻¹, with an incubation time of 2 min, and subsequently washed twice in a cell imaging medium.

Cellular mitochondria: Mitochondria were fluorescently labeled using MitoTracker Red CM-H$_2$XRos (M7513, Thermo Fisher Scientific) at a concentration of 400 nm (prepared in the full F-12K cell culture medium) and with an incubation time of 45 min (at 37 °C, 5% CO$_2$). Cells were subsequently washed in the cell imaging medium. Cells were then stained for their nuclei as above.

Indirect Immunofluorescence Labeling of Fixed Cells: The nuclei of A549 cells were stained by incubating them in Hoechst33342 (Thermo Fisher Scientific) at a concentration of 2.5 µg ml⁻¹ in a cell imaging medium for 2 min at room temperature and in the dark. Cells were washed twice in a cell imaging medium for 2 min. Cells were subsequently fixed with 4% paraformaldehyde (158127, Sigma-Aldrich via Merck) in PBS for 10 min at room temperature and washed twice with PBS for 5 min. Cells were incubated with 0.25% Triton X-100 (X100, Sigma-Aldrich via Merck) in PBS for 10 min for permeabilization and were subsequently incubated in 2% BSA (A1933, Sigma-Aldrich via Merck) in PBS for 10 min for blocking, then washed twice with PBS for 5 min. Cells were incubated for 1 h at room temperature in the dark with primary antibody targeting lysosomes (rabbit anti-LAMP1, PA1-654A, Invitrogen via ThermoFisher Scientific;

used at a concentration of 2 µg ml⁻¹ in PBS with 2% BSA). Samples were washed twice in PBS for 5 min. Samples were then incubated for 1 h at room temperature in the dark with the secondary antibody goat anti-rabbit-STAR580 (Abberior GmbH) at 2 µg ml⁻¹. After incubation with the secondary antibody, samples were washed twice in PBS for 5 min and then mounted in Abberior Mount Liquid Antifade (MM-2009-2 × 15 mL, Abberior GmbH) onto a glass-bottom Petri dish (P35G-1.5-20-C, MatTek Corporation, Ashland, MA, USA; with cells facing the glass-bottom of the dish). The mounted samples were left to harden overnight, sealed with clear nail polish, and imaged within 5 days after preparation.

Confocal and STED Imaging: All live-cell imaging was performed in cell imaging medium. Cells grown and stained on the glass-bottom Petri dishes were directly imaged in the petri dishes; cells grown and treated in nanostraw devices were imaged after gently peeling off the nanostraw membrane from the plastic cylinder and placing it upside-down inside a drop of cell imaging medium on a glass cover slip inside a microscope stage cell incubator (POC-R2, PeCon GmbH, Erbach, Germany), while making sure there was no pressure applied to the cells. By altering the amount of cell imaging medium into which the cells on the nanostraw membrane were placed, a distance of 2–10 µm between the apical cell membrane and the cover slip could be maintained during confocal imaging.

Fluorescence microscopy images were obtained using the STED microscope system Abberior 2C STED 775 QUAD Scan (Abberior Instruments GmbH, Goettingen, Germany), operated in either confocal or STED mode. The intracellular FND signal was recorded in confocal mode using the 561 nm excitation laser and a (685/70) nm detection window; the lysosome signal was recorded in confocal mode using the 561 nm excitation laser and a (605/50) nm detection window. For two-color STED images of live cells incubated with FND via the cell medium and subsequently stained for lysosomes, the intracellular FND signal was recorded using the 561 nm excitation laser, the 775 nm STED laser, and a (685/70) nm detection window; the lysosome signal was recorded using the 561 nm excitation laser, the 775 nm STED laser, and a (605/50) nm detection window. The two-color STED images were acquired using line-interleaved, simultaneous scanning. The cell nucleus signal was recorded in confocal mode using the 405 nm excitation laser and a (450/50) nm detection window. The cellular membrane signal was recorded in STED mode using the 640 nm excitation laser, the 775 nm STED laser, and a (685/70) nm detection window. Laser powers were kept constant for individual experiments using the microscope software control and corresponded to 40% of the maximum power for the 561 nm excitation laser (corresponding to 20 µW, as measured in the back focal plane of the objective and 18 µW when taking into account the transmittance of 90% of the microscope objective Nikon CFI Plan Apochromat Lambda 60X Oil NA 1.40 at the wavelength of 561 nm), 30% of the maximum power for the 640 nm excitation laser (corresponding to 37 µW, as measured in the back focal plane of the objective, and 31.5 µW when taking into account the transmittance of 85% of the microscope objective at the wavelength of 640 nm), 100% of the maximum power for the 775 nm STED laser (corresponding to 90 mW, as measured in the back focal plane of the objective, and 67.5 mW taking into account the transmittance of 75% of the microscope objective at the wavelength of 775 nm), and 2% of the maximum power for the 405 nm excitation laser (corresponding to 27 µW, as measured in the back focal plane of the objective, and 16 µW taking into account the transmittance of 60% of the microscope objective at the wavelength of 405 nm). All images were obtained using a pinhole size of 1.7 Airy units (AU) with an associated Depth of Field (DOF) of 0.945 µm (according to $DOF = \frac{\lambda * n}{(NA)^2} + \frac{n}{M * NA} * e$, with λ denoting the excitation wavelength and assumed to be of an average of 600 nm in this study, n denoting the index of refraction of the used immersion oil (n = 1.515), *NA* denoting the numerical aperture of the used objective (NA = 1.40), M denoting the magnification of the used objective (M = 60), and e denoting the resolution of a detector placed in the image plane of the microscope and in this case corresponding to the radius of the confocal pinhole).

Multi-color images were recorded in line-interleaved mode with a single line accumulation and a pixel dwell time of 5 µs. For all live

**ADVANCED
SCIENCE NEWS**

www.advancedsciencenews.com

NANO · MICRO
small

www.small-journal.com

cell images, 2D confocal images were obtained with a pixel size of (50×50) nm^2; 2D STED images were obtained with a pixel size of (20×20) nm^2. Z-stack images of fluorescence labeled cells were obtained with voxel sizes of $(70 \times 70 \times 250)$ nm^3.

Live Cell Membrane STED Microscopy Imaging during Low Voltage Electroporation: For the acquisition of video-rate STED images of the membrane of cells on nanostraws during the low-voltage electroporation step, cells were cultured on inverted PET nanostraw devices (i.e., with nanostraws protruding away from the plastic cylinders) for 18 h. Subsequently, the inverted nanostraw devices were mounted in a drop of ca. 20 µl cell imaging medium on an indium tin oxide (thickness 20 nm) coated cover slip on the STED microscope stage, making sure not to apply pressure to the cells. See Figure S9, Supporting Information, for schematics of the experimental setup. Two sets of experiments were performed: One where the focus was adjusted to the tip of the nanostraws and one where the focus was adjusted to the middle of the nanostraws. In order to ensure a stable focal imaging plane and to correct for potential drift of the sample in the axial direction, the perfect focus function of the STED microscope was activated during video rate scanning. In order to set the focus on the top of the nanostraws, we scrolled through the cells from the bottom of the cell and stopped when first detecting the membrane on the nanostraw signal. Then we used the focus lock of the microscope (Nikon Eclipse TE2000). In order to set the focus at the nanostraw mid-height, we measured the z coordinates from the top of the nanostraws and stopped at the middle of the length, which we know from SEM measurements. The membrane signal was imaged using a pixel size of (20×20) nm^2, with a pixel dwell time of 2 µs and ROI sizes resulting in a frame rate of about 1 fps; 5 s after the start of the scan, the electric field (square electrical pulses, 25 V, 20 Hz, 100 µs pulse duration), was switched on for 30 (focus on top of the nanostraws) and 20 s (focus on the middle of the nanostraws). The cell membrane was imaged for 110 s (focus on top of the nanostraws) and 10 s (focus on the middle of the nanostraws) after switching off the electric field. For imaging the recovery of the membrane, the membrane signal on top of the nanostraws was imaged using a pixel size of (20×20) nm^2, with a pixel dwell time of 5 µs, before and during the electrical pulse application (square electrical pulses, 25 V, 20 Hz, 100 µs pulse duration, applied for 20 s), as well as every 5 min after switching off the electrical pulses.

Image Analysis: All acquired images were visualized, processed, and analyzed using ImSpector, Fiji (http://imagej.net/Fiji) and MATLAB (The MathWorks, Inc., Natick, Massachusetts, United States). Image smoothing was performed with the ImSpector software using a low-pass Gaussian filter with a width of 1.5 times the respective image pixel size (typically corresponding to 30 nm). If a smoothing step has been applied to the images, it is stated explicitly in the corresponding figure caption.

For image display, the image brightness was normalized to the measured photon counts per pixel as recorded by the ImSpector software; in some cases, a subtraction of noise was performed. The image brightness, normalized based on pixel photon counts, is given explicitly for each image displayed in the figures herein.

Images displaying the maximum pixel brightness projection (denoted as "maximum projection" in the respective figures and images) were generated from recorded axial scans (Z-stacks) of the samples using ImSpector. Histograms of image pixel brightness distributions were generated using ImSpector. The integrated pixel intensities of the FND shown in Figure 2 were determined by the summation of all the pixel photon counts of the background-corrected individual images. The integrated pixel intensity in each image was normalized to the total cell surface area determined from the corresponding brightfield image (determined from cell segmentation after identifying the cellular outlines using the software Fiji). The data in Figure 2c was calculated by considering a minimum of 70 cells per treatment (incubation for 1 h, incubation for 24 h, and 5 min after nanostraw-assisted injection), which were taken from five independent experimental repeats.

Two-color images generated from the overlay of the nanodiamond and lysosome signal, acquired in two separate detection channels of the

confocal/STED microscope, were converted to a color map comprising zero signal in black, the first color channel in cyan, the second color channel in magenta, and overlap of the two color channels in yellow. The color channel brightness was normalized to its respective minimum and maximum.

For the assessment of the relative colocalization of red FND and lysosomes (labeled via LAMP1), each single color channel composing the confocal images (FND and LAMP1) was corrected for fluorescence background signal and spectral crosstalk, then a threshold was applied to the image's maximum pixel brightness. The images were then binarized using a custom-written MATLAB routine. In detail, fluorescence background correction was performed by a per-pixel subtraction of a constant pixel count value, which was assessed as the maximum pixel count in an image area free of any cellular structure. This correction value was determined individually for each single color channel in each acquired image. Spectral crosstalk correction was performed by using control samples that were positive for only FND or only LAMP1, and that had undergone the same cell culture steps as their multi-color counterparts. From these single-color samples, the fraction of fluorescence signal in the crosstalk channel versus fluorescence signal in the true color channel was assessed and extracted pixel-by-pixel. The average fraction f_{CT} of the respective FND or LAMP1-STAR580 spectral crosstalk under different sample treatment conditions was then used for crosstalk correction of the images of the corresponding dual-labeled samples: if a pixel i showed positive signal S_i in both color channels, its value $S_{i,Red}$ in the red channel was reduced to $(1 - f_{CT,Green})*S_{i,Red}$ and its value $S_{i,Green}$ in the green channel was reduced to $(1 - f_{CT,Red})*S_{i,Green}$ to account for the spectral signal overlap (with $f_{CT,Green}$ and $f_{CT,Red}$ denoting the extracted spectral crosstalk fraction of the green signal into the red channel and the red signal into the green channel, respectively). For clarity purposes, a flow chart of the image analysis process is available in the Supporting Information (Figure S10, Supporting Information). Note that, despite an overlap of the FND emission spectrum with the green detection channel, the FND (red) signal was not detected in the green channel (Figure S11, Supporting Information). For setting the threshold of signal brightness in the images, a pixel was considered a "positive signal" if its brightness accounted to at least 7% of the maximum image brightness and if it was surrounded by neighboring pixels of at least 5% of the maximum image brightness. Binarized images were converted into a false color scheme with the FND positive signal in red and the LAMP1 positive signal in green. Overlay of the binarized and color-converted images resulted in yellow FND and LAMP1 positive pixels and in black FND and LAMP1 negative pixels. From the overlay images, the relative colocalization of one single-color channel with the other single-color channel was determined by dividing the number of pixels positive for both channels by the total number of pixels in the respective single color channel. This relative colocalization (%) thus describes the ratio of the signal of the first color signal colocalizing with the second color signal with respect to the total signal of the first color channel.

The resolution of signal structures was determined by plotting the summed-up pixel intensity profile of the signal against its position along a line of the thickness of 3px and by fitting a Gaussian function to the obtained intensity distribution. The upper limit of the image resolution was determined from these fits as the full width at half maximum of the Gaussian fit curve.

Numerical Simulations of Two-Color FND and LAMP1-STAR580 Signal for Random Colocalization: To estimate the statistical significance of the determined relative colocalization between the FND signal and LAMP1-STAR580 signal (data presented in Figure 3) for different FND delivery scenarios (1 h incubation, 24 h incubation, 1 h after nanostraw-assisted injection, and 24 h after nanostraw-assisted injection), we simulated the mean relative colocalization in case of a completely random signal distribution in each color channel. For this, we assessed the total number of FND-positive ("red") signal pixels and LAMP1-STAR580-positive ("green") signal pixels for each acquired two-color fluorescence image (after background and crosstalk correction, as described above). These pixels were then randomly distributed within a 2D grid with the same pixel

dimensions as the underlying experimentally recorded fluorescence image. The coordinates of the randomly distributed "red" and "green" pixels were compared and matching coordinate pairs were counted as overlapping ("yellow") pixels. The random relative colocalization was determined as the percentage of random "yellow" pixels out of the number of all "red" pixels and is displayed as mean ± S.E.M. in Figure S6, Supporting Information (in direct comparison to the relative colocalization of the experimental data presented in Figure 3). The statistical significance of the relative colocalization of the real versus simulated data was assessed using the two-sided Mann–Whitney–Wilcoxon U-test.

The simulation procedure was carried out in MATLAB using a custom-written script and by employing MATLAB's built-in random number generation function ("rand()") in order to generate randomly distributed pixel coordinates within the dimensions of the corresponding experimentally acquired two-color fluorescence image.

Statistical Significance Testing: Five independent replicates of each injection/incubation experiment were performed. A minimum of 18 images were analyzed for each treatment. Statistical significance of the data was tested using the two-sided Mann–Whitney–Wilcoxon U test using the MATLAB script "mwwtest.m".[57]

Supporting Information

Supporting Information is available from the Wiley Online Library or from the author.

Conflict of Interest

Martin Hjort is Chief Technology Officer at Navan Technologies, Inc., a startup commercializing nanostraws.

Data Availability Statement

Data available on request from the authors. The data that support the findings of this study are available from the corresponding author upon reasonable request.

[1] B. M. Chang, H. H. Lin, L. J. Su, W. Der Lin, R. J. Lin, Y. K. Tzeng, R. T. Lee, Y. C. Lee, A. L. Yu, H. C. Chang, *Adv. Funct. Mater.* **2013**, *23*, 5737.

[2] M. H. Alkahtani, F. Alghannam, L. Jiang, A. Almethen, A. A. Rampersaud, R. Brick, C. L. Gomes, M. O. Scully, P. R. Hemmer, *Nanophotonics* **2018**, *7*, 1423.

[3] M. Chipaux, K. J. van der Laan, S. R. Hemelaar, M. Hasani, T. Zheng, R. Schirhagl, *Small* **2018**, *14*, 1704263.

[4] G. Kucsko, P. C. Maurer, N. Y. Yao, M. Kubo, H. J. Noh, P. K. Lo, H. Park, M. D. Lukin, *Nature* **2013**, *500*, 54.

[5] T. J. Wu, Y. K. Tzeng, W. W. Chang, C. A. Cheng, Y. Kuo, C. H. Chien, H. C. Chang, J. Yu, *Nat. Nanotechnol.* **2013**, *8*, 682.

[6] K. K. Liu, C. C. Wang, C. L. Cheng, J. I. Chao, *Biomaterials* **2009**, *30*, 4249.

[7] D. A. Simpson, E. Morrisroe, J. M. McCoey, A. H. Lombard, D. C. Mendis, F. Treussart, L. T. Hall, S. Petrou, L. C. L. Hollenberg, *ACS Nano* **2017**, *11*, 12077.

[8] F. J. Hsieh, S. Sotoma, H. H. Lin, C. Y. Cheng, T. Y. Yu, C. L. Hsieh, C. H. Lin, H. C. Chang, *ACS Appl. Mater. Interfaces* **2019**, *11*, 19774.

[9] R. Igarashi, T. Sugi, S. Sotoma, T. Genjo, Y. Kumiya, E. Walinda, H. Ueno, K. Ikeda, H. Sumiya, H. Tochio, Y. Yoshinari, Y. Harada, M. Shirakawa, *J. Am. Chem. Soc.* **2020**, *142*, 7542.

[10] C. P. Epperla, N. Mohan, C. W. Chang, C. C. Chen, H. C. Chang, *Small* **2015**, *11*, 6097.

[11] T. Zheng, F. Perona Martínez, I. M. Storm, W. Rombouts, J. Sprakel, R. Schirhagl, R. De Vries, *Anal. Chem.* **2017**, *89*, 12812.

[12] O. Faklaris, V. Joshi, T. Irinopoulou, P. Tauc, M. Sennour, H. Girard, C. Gesset, J. C. Arnault, A. Thorel, J. P. Boudou, P. A. Curmi, F. Treussart, *ACS Nano* **2009**, *3*, 3955.

[13] S. Han, M. Raabe, L. Hodgson, J. Mantell, P. Verkade, T. Lasser, K. Landfester, T. Weil, I. Lieberwirth, *Nano Lett.* **2019**, *19*, 2178.

[14] Y. Wu, A. Ermakova, W. Liu, G. Pramanik, T. M. Vu, A. Kurz, L. McGuinness, B. Naydenov, S. Hafner, R. Reuter, J. Wrachtrup, J. Isoya, C. Förtsch, H. Barth, T. Simmet, F. Jelezko, T. Weil, *Adv. Funct. Mater.* **2015**, *25*, 6576.

[15] S. R. Hemelaar, P. De Boer, M. Chipaux, W. Zuidema, T. Hamoh, F. Perona Martinez, A. Nagl, J. P. Hoogenboom, B. N. G. Giepmans, R. Schirhagl, *Sci. Rep.* **2017**, *7*, 720.

[16] S. Haziza, N. Mohan, Y. Loe-Mie, A. M. Lepagnol-Bestel, S. Massou, M. P. Adam, X. L. Le, J. Viard, C. Plancon, R. Daudin, P. Koebel, E. Dorard, C. Rose, F. J. Hsieh, C. C. Wu, B. Potier, Y. Herault, C. Sala, A. Corvin, B. Allinquant, H. C. Chang, F. Treussart, M. Simonneau, *Nat. Nanotechnol.* **2017**, *12*, 322.

[17] L. Marcon, F. Riquet, D. Vicogne, S. Szunerits, J. F. Bodart, R. Boukherroub, *J. Mater. Chem.* **2010**, *20*, 8064.

[18] Y. Kuo, T. Y. Hsu, Y. C. Wu, H. C. Chang, *Biomaterials* **2013**, *34*, 8352.

[19] D. A. Simpson, A. J. Thompson, M. Kowarsky, N. F. Zeeshan, M. S. J. Barson, L. T. Hall, Y. Yan, S. Kaufmann, B. C. Johnson, T. Ohshima, F. Caruso, R. E. Scholten, R. B. Saint, M. J. Murray, L. C. L. Hollenberg, *Biomed. Opt. Express* **2014**, *4*, 1250.

[20] Y. C. Lin, K. T. Wu, Z. R. Lin, E. Perevedentseva, A. Karmenyan, M. D. Lin, C. L. Cheng, *J. Biophotonics* **2016**, *9*, 827.

[21] O. Loh, R. Lam, M. Chen, N. Moldovan, H. Huang, D. Ho, H. D. Espinosa, *Small* **2009**, *5*, 1667.

[22] Z. Chu, S. Zhang, B. Zhang, C. Zhang, C. Y. Fang, I. Rehor, P. Cigler, H. C. Chang, G. Lin, R. Liu, Q. Li, *Sci. Rep.* **2014**, *4*, 4495.

[23] Z. Chu, K. Miu, P. Lung, S. Zhang, S. Zhao, H. C. Chang, G. Lin, Q. Li, *Sci. Rep.* **2015**, *5*, 11661.

[24] M. A. Zurbuchen, M. P. Lake, S. A. Kohan, B. Leung, L. S. Bouchard, *Sci. Rep.* **2013**, *3*, 2668.

[25] M. P. Lake, L. S. Bouchard, *PLoS One* **2017**, *12*, e0179295.

[26] A. Janaszewska, K. McZyńska, G. Matuszko, D. Appelhans, B. Voit, B. Klajnert, M. Bryszewska, *New J. Chem.* **2012**, *36*, 428.

[27] Y. K. Tzeng, O. Faklaris, B. M. Chang, Y. Kuo, J. H. Hsu, H. C. Chang, *Angew. Chem., Int. Ed.* **2011**, *50*, 2262.

[28] S. R. Hemelaar, K. J. Van Der Laan, S. R. Hinterding, M. V. Koot, E. Ellermann, F. P. Perona-Martinez, D. Roig, S. Hommelet, D. Novarina, H. Takahashi, M. Chang, R. Schirhagl, *Sci. Rep.* **2017**, *7*, 5862.

[29] J. J. VanDersarl, A. M. Xu, N. A. Melosh, *Nano Lett.* **2012**, *12*, 3881.

[30] L. Schmiderer, A. Subramaniam, K. Žemaitis, A. Bäckström, D. Yudovich, S. Soboleva, R. Galeev, C. N. Prinz, J. Larsson, M. Hjort, *Proc. Natl. Acad. Sci. USA* **2020**, *117*, 21267.

[31] X. Xie, A. M. Xu, S. Leal-Ortiz, Y. Cao, C. C. Garner, N. A. Melosh, *ACS Nano* **2013**, *7*, 4351.

[32] Y. Cao, H. Chen, R. Qiu, M. Hanna, E. Ma, M. Hjort, A. Zhang, R. S. Lewis, J. C. Wu, N. A. Melosh, *Sci. Adv.* **2018**, *4*, eaat8131.

[33] A. Tay, N. Melosh, *Adv. Ther.* **2019**, *2*, 1900133.

[34] S. Arroyo-Camejo, M. P. Adam, M. Besbes, J. P. Hugonin, V. Jacques, J. J. Greffet, J. F. Roch, S. W. Hell, F. Treussart, *ACS Nano* **2013**, *7*, 10912.

[35] S. R. Hemelaar, A. Nagl, F. Bigot, M. M. Rodríguez-García, M. P. de Vries, M. Chipaux, R. Schirhagl, *Microchim. Acta* **2017**, *184*, 1001.

[36] M. P. Stewart, A. Lorenz, J. Dahlman, G. Sahay, *Wiley Interdiscip. Rev.: Nanomed. Nanobiotechnol.* **2016**, *8*, 465.

[37] D. Pei, M. Buyanova, *Bioconjugate Chem.* **2019**, *30*, 273.

[38] W. J. Rhee, G. Bao, *Nucleic Acids Res.* **2010**, *38*, e109.

[39] S. Chikte, N. Panchal, G. Warnes, *Cytometry, Part A* **2014**, *85*, 169.

[40] S. R. Tabaei, M. Rabe, V. P. Zhdanov, N. J. Cho, F. Hook, *Nano Lett.* **2012**, *12*, 5719.

[41] A. M. Xu, A. Aalipour, S. Leal-Ortiz, A. H. Mekhdjian, X. Xie, A. R. Dunn, C. C. Garner, N. A. Melosh, *Nat. Commun.* **2014**, *5*, 3613.

[42] X. Xie, A. Aalipour, S. V. Gupta, N. A. Melosh, *ACS Nano* **2015**, *9*, 11667.

[43] A. Honigmann, V. Mueller, H. Ta, A. Schoenle, E. Sezgin, S. W. Hell, C. Eggeling, *Nat. Commun.* **2014**, *5*, 5412.

[44] E. Sezgin, F. B. Can, F. Schneider, M. P. Clausen, S. Galiani, T. A. Stanly, D. Waithe, A. Colaco, A. Honigmann, D. Wüstner, F. Platt, C. Eggeling, *J. Lipid Res.* **2016**, *57*, 299.

[45] C. Xie, Z. L. Lin, L. Hanson, Y. Cui, B. X. Cui, *Nat. Nanotechnol.* **2012**, *7*, 185.

[46] G. Saulis, R. Saule, *Biochim. Biophys. Acta, Biomembr.* **2012**, *1818*, 3032.

[47] P. Mukherjee, S. S. P. Nathamgari, J. A. Kessler, H. D. Espinosa, *ACS Nano* **2018**, *12*, 12118.

[48] S. S. P. Nathamgari, N. Pathak, V. Lemaitre, P. Mukherjee, J. J. Muldoon, C. Peng, T. McGuire, J. N. Leonard, J. A. Kessler, H. D. Espinosa, *Small* **2020**, *16*, 2002616.

[49] M. P. Rols, J. Teissié, *Biophys. J.* **1998**, *75*, 1415.

[50] X. Xie, A. M. Xu, M. R. Angle, N. Tayebi, P. Verma, N. a. Melosh, *Nano Lett.* **2013**, *13*, 6002.

[51] A. K. Shalek, J. T. Robinson, E. S. Karp, J. S. Lee, D.-R. Ahn, M.-H. Yoon, A. Sutton, M. Jorgolli, R. S. Gertner, T. S. Gujral, G. MacBeath, E. G. Yang, H. Park, *Proc. Natl. Acad. Sci. USA* **2010**, *107*, 1870.

[52] T. Berthing, S. Bonde, K. R. Rostgaard, M. H. Madsen, C. B. Sorensen, J. Nygard, K. L. Martinez, *Nanotechnology* **2012**, *23*, 415102.

[53] L. Hanson, Z. C. Lin, C. Xie, Y. Cui, B. Cui, *Nano Lett.* **2012**, *12*, 5815.

[54] H. Persson, C. Købler, K. Mølhave, L. Samuelson, J. O. Tegenfeldt, S. Oredsson, C. N. Prinz, *Small* **2013**, *9*, 4006.

[55] F. Santoro, S. Dasgupta, J. Schnitker, T. Auth, E. Neumann, G. Panaitov, G. Gompper, A. Offenhäusser, *ACS Nano* **2014**, *8*, 6713.

[56] L. Abariute, M. Lard, E. Hebisch, C. N. Prinz, *PLoS One* **2019**, *14*, e0218122.

[57] G. Cardillo, https://se.mathworks.com/matlabcentral/fileexchange/25830-mwwtest (accessed: April 2020).